processes

MDPI

Article

Stress Zoning Characteristics and Migration of Leaked Methane from Gas Wells Penetrating Protective Coal Pillars in Longwall Mining Areas

Jinhang Shen [1], Shun Liang [1,*], Yisong Hao [2], Zhi Ma [3], Weisheng He [3], Xu Liang [4], Shaoyou Xu [5] and Changheng Luo [5]

[1] State Key Laboratory for Fine Exploration and Intelligent Development of Coal Resources, China University of Mining and Technology, Xuzhou 221116, China
[2] Shaqu No. 2 Mine Huajin Coking Corporation Limited, Lvliang 033301, China
[3] Ningxia Coal Industry Limited Liability Company Shuangma Coal Mine, China Energy Group, Yinchuan 750408, China
[4] Shaanxi Xiaobaodang Mining Corporation Limited, Yulin 719302, China
[5] No. 2 Gas Production Plant of Sinopec North China Oil and Gas Company, Ordos 017400, China
* Correspondence: 5756@cumt.edu.cn; Tel.: +86-151-6212-4780

Abstract: There are a large number of abandoned or casing-damaged oil/gas wells in the western mining areas of China. Under the influence of mining-induced stress, the methane leaked from the oil and gas wells will be transported through fracture within the coal pillar to the longwall working face, which will seriously threaten the safe mining of coal resources. There is no mandatory standard for the practice of coal pillars in coal and gas wells in coal/gas overlapping areas, and the problems of oversized coal pillars and waste of coal resources have occurred during the implementation. In this study, through finite element numerical simulation, three different sizes of protective coal pillars are modeled in the background of Shuangma Coal Mine. The impacts of different heights and widths of protective coal pillars on the evolution of stresses and the diffusion process of leaked methane are explored, and the spatial and temporal migration law of leaked methane under multi-field coupling is revealed. The results show that under mining-induced stress, the size of the protective coal pillar has a significant effect on the stress distribution and methane transport law. Compared with the 130 m coal pillar, the peak stress of the 150 m coal pillar decreased by 6.7%, and the peak stress of the 180 m coal pillar decreased by 9%. At 150 m and 180 m widths, the permeability difference between the two sides is only 1 mD, and the diffusion ranges are similar. From the stress distribution and gas diffusion law, it is shown that the effect achieved by 150 m and 180 m coal pillars is similar. This work is of great significance for the reasonable remaining protective coal pillars for oil/gas wells penetrating longwall mining areas, as well as the prevention and control of disasters caused by leaked methane from wells.

Keywords: abandoned oil/gas wells; mining stress; protective coal pillars; leaked methane

check for updates

Academic Editor: Carlos Sierra Fernández

Received: 25 November 2024
Revised: 20 December 2024
Accepted: 24 December 2024
Published: 28 December 2024

Citation: Shen, J.; Liang, S.; Hao, Y.; Ma, Z.; He, W.; Liang, X.; Xu, S.; Luo, C. Stress Zoning Characteristics and Migration of Leaked Methane from Gas Wells Penetrating Protective Coal Pillars in Longwall Mining Areas. *Processes* **2025**, *13*, 47. https://doi.org/10.3390/pr13010047

Copyright: © 2024 by the authors. Licensee MDPI, Basel, Switzerland. This article is an open access article distributed under the terms and conditions of the Creative Commons Attribution (CC BY) license (https://creativecommons.org/licenses/by/4.0/).

1. Introduction

As coal resources in eastern China gradually decreased, coal mining progressively shifted to the western regions of China. The engineering practices of coal–oil or coal–gas cross-exploitation are becoming more common, particularly in the Ordos, Junggar, and Tarim Basins [1–3]. These practices encounter many problems. Due to the early development of resources such as oil and gas, more and more production wells are in the late

stage, leaving a large number of abandoned wells, which contain a large amount of natural gas, associated gas, as well as toxic and harmful gases such as carbon monoxide and methane [4,5]. These abandoned wells remaining from the early stage, due to the lack of casing or damage caused by aging, have led to the diffusion of toxic and harmful gases from the oil/gas wells into coal seams and even the atmosphere, seriously threatening coal mining safety and the surrounding ecosystem. This not only means a huge waste of resources but also brings many hazards to nearby coal seams mining [6–8]. Therefore, in these areas, maintaining the stability of wells in the longwall mining area is key to the safe mining adjacent coal seams [9–12].

Literature research reveals limited research on the stability of oil/gas wells affected by coal seam mining in common engineering practices, and no specific standards exist for remaining coal pillars in oil/gas wells [13]. Previous studies have focused on factors such as coal seam burial depth, mining-induced stress, coal pillar dimensions, and the relative position relationship between the well and the working face in the design of gas well protective pillars. As engineering practices increase, previous researchers have further pointed out that the horizontal and shear movements of strata caused by mining significantly impact the deformation of wells. The response modes of each stratum to horizontal and shear movements are different, resulting in the inconsistency of deformation between adjacent strata. This inconsistency in deformation can easily lead to shear deformation of the wellbore. Liang Shun et al. explored the distribution of axial stress, strain, and displacement in oil/gas wells under various factors, identifying the timing and layers where wells are most susceptible to destabilization. The goal is to focus on protecting these unstable areas and preventing instability and leakage in oil/gas wells during longwall mining [9,14,15]. However, most research has centered on the casing stability of wells, with limited focus on the safety of wells lacking casing or damaged due to aging.

In the coalbed methane field, scholars such as Gray, Bustin, and Cui [16–18] assume that the overburden stress of the coal seam is constant and the stress on the coal mass is uniform. By constructing different variables, they propose a classical permeability model, which is significant for studying CBM exploitation and methane migration from abandoned oil/gas wells. Subsequent scholars [19,20] studied the impact of oil and gas pipeline leaks on methane diffusion in shallow aquifers using methods such as multiphase, multi-component, and numerical models. They believed that factors such as geological conditions, phase behavior, and coal seam dip angle affect methane permeability, which in turn influences the diffusion range of methane. Krzysztof Skrzypkowski [21] used a number of experiments to show that cracked rocks are particularly susceptible to gas migration, which translates into a weakening of strength and deformation parameters.

In summary, previous studies on deformation, instability, and leakage in wells during the co-extraction of coal, oil, and gas resources have mostly focused on situations where the well casing is intact and there is no leakage. There is little research on the safety of oil/gas wells that have not been cased or have been damaged due to age. The study of methane migration often adopts the assumption of uniform stress, focusing on the impact of oil/gas pipeline leaks on methane diffusion in shallow aquifers. However, in the coal-oil–gas overlapping zone, the mining of the working face will cause the stress on the coal mass to be unbalanced, and previous studies have not considered the stress evolution caused by coal seam mining. Therefore, this study takes Shuangma Coal Mine's remaining protective coal pillars as the engineering background, considering the effects of mining-induced stress and casing damage on both the stability of wells and the design of protective coal pillars, and carries out the evolution of mining-induced stress and migration of leaked methane from gas wells penetrating protective coal pillars. The results of the study are of great significance for optimizing the size of protective coal pillars in oil/gas wells without casing

or damaged due to age in longwall mining areas, improving the recovery rate of coal resources, revealing the mechanism of underground disasters caused by leaked methane from oil/gas wells, and realizing safe and efficient mining of coal, oil, and gas resources.

2. Characteristics of Stress Evolution Within Protective Coal Pillars for Gas Wells

The coal pillar is an enclosed, non-visible space, making it challenging to accurately monitor the evolution of the stress field within protective coal pillars of gas wells during mining due to technical and site limitations. Therefore, based on FLAC3D 6.0 simulation software and the actual working conditions of Shuangma Coal Mine, this study analyzes the stress evolution within coal pillars of varying widths and heights and its effects on the stability and deformation of gas wells, as well as their effects on the bearing and deformation of gas wells inside the coal pillar.

2.1. Engineering Geology Conditions

The Shuangma Coal Mine is located in the Ordos Basin, with an area of approximately 67.99 km^2 and an annual output of 4 Mt. It mines the 4 # coal seam and uses the caving method for roof management. There are small faults in the coal mine working face, but they do not affect normal mining operations. Overall, the geological structure of Shuangma Coal Mine is simple. More than 170 oil/gas wells have been explored in Shuangma Coal Mine, which has caused serious safety problems for the mining face. The main coal seam, the 4^{-1} seam, has a simple geological structure and a mining face length of 280 m. It includes one abandoned gas well without safety measures, where gas pressure ranges from 9 to 15 MPa. The average thickness of the coal seam is 4 m, and its burial depth is 290 m; vertical stress is 6.9 Mpa, and horizontal stress is 8.28 Mpa. As shown in Figure 1, the seam roof is primarily fine sandstone, while the floor is predominantly mudstone.

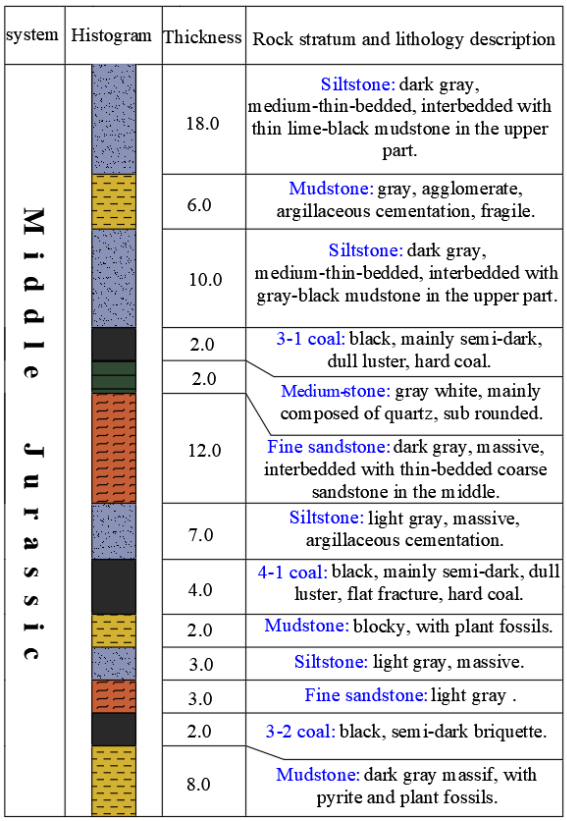


Figure 1. Histogram of the coal seam of Shuangma Coal Mine.

2.2. Distribution Characteristics of Stress Within Different Dimensional Protective Coal Pillars for Gas Wells

2.2.1. Simulation Scenario

Based on the geological conditions of Shuangma Coal Mine, and referencing coal mining methods used under buildings and protective coal pillar dimensions designed for oil/gas wells in similar mines, the protective coal pillar width is designed at 180 m in Shuangma; this method has a large margin coefficient, so three different pillar schemes were designed with a maximum boundary of 180 m, namely 130 m, 150 m, and 180 m. This study uses FLAC numerical simulation to create the geological and Mohr-Coulomb models to simulate rock formations. Physical and mechanical parameters are listed in Table 1. The lower boundary is constrained in the model, while the front-back and left-right boundaries restrict displacement in the Z, X, and Y directions, respectively; the upper surface remains free. The mining sequence follows site operations: the left working face is mined first, followed by the right working face. The specific model parameters are illustrated in Figure 2. Figure 3 presents the xz-plane section of the model. Figure 3a illustrates schemes with varying widths of coal pillars, where different advancement stages represent the retention of coal pillars with different widths. For instance, when the working face advances to position III, it signifies the retention of a coal pillar with a width of 180 m. Figure 3b depicts schemes with varying heights of coal pillars, where different mining heights represent the retention of coal pillars with different heights. For example, when the mining height is 1 m, the height of the retained coal pillar is 1 m.

Table 1. Physical and mechanical parameters of rock lithologies employed in numerical simulation.

Lithology	Density (Kg/m^3)	Bulk (GPa)	Shear (GPa)	Cohesion (MPa)	Tension (MPa)	Friction (°)
Medium-sandstone	2550	4.63	2.40	1.9	1.5	30.2
Mudstone	2430	3.5	1.85	1.2	0.8	25.1
Fine-sandstone	2620	5.32	2.98	1.7	1.3	28.0
Siltstone	2600	4.30	2.38	1.4	0.9	28
coal	1400	2.89	1.83	0.8	0.6	20.4

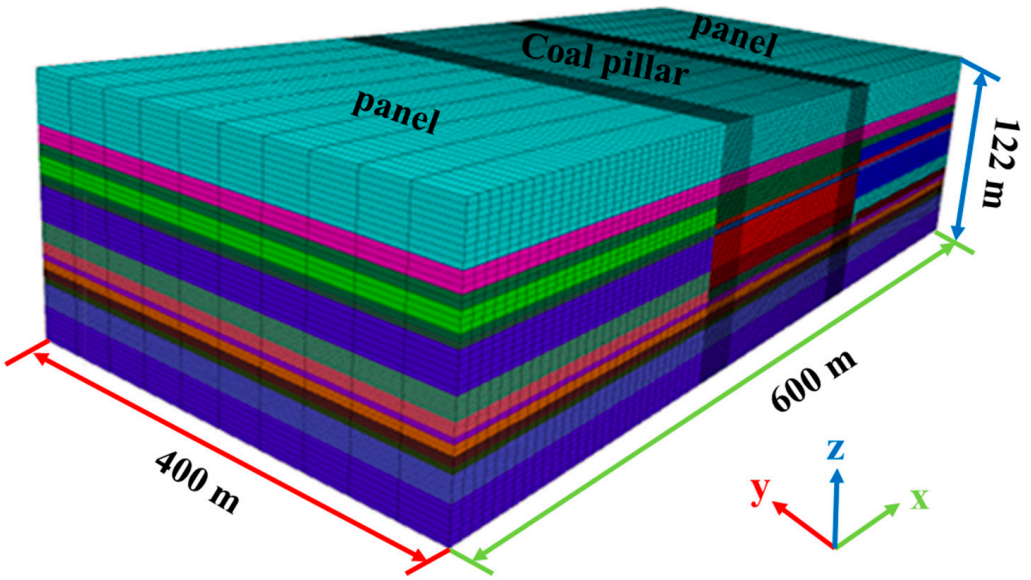


Figure 2. FLAC3D geological model.

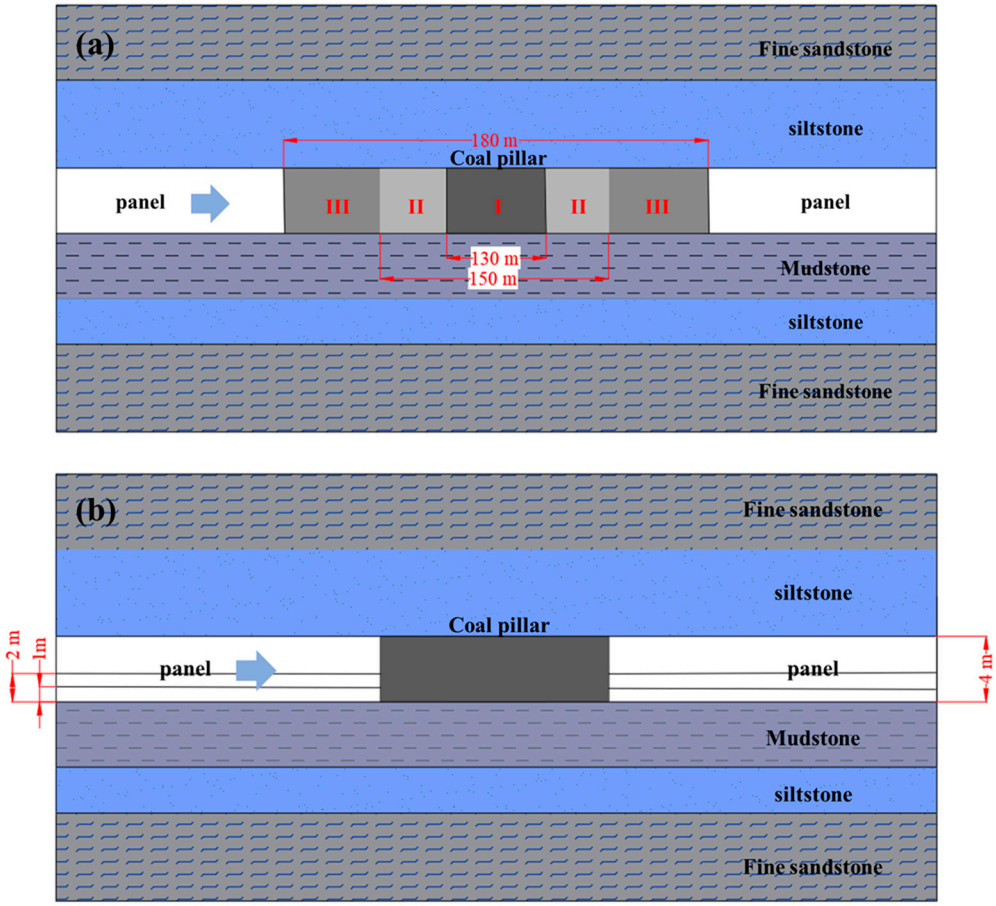


Figure 3. Schematic diagram of the simulation scheme ((**a**) schemes of varying widths (**b**) schemes of varying heights).

2.2.2. Simulation Results and Analysis

The vertical stress within the coal pillar is symmetrically distributed, forming a 'saddle' shape (Figure 4). As the working face advances, the roof forms a 'bottom-shaped' structure, and both sides of the pillar are subject to bearing pressure; the vertical stress increases, and the closer to the middle, the vertical stress decreases. When one side of the working face is mined, the coal pillar is subjected to mining-induced stress, leading to a redistribution of stress within the coal pillar ahead of the working face. Specifically, the vertical stress near the working face increases while the vertical stress farther from the working face decreases. The peak stress and influence range of protective coal pillars with different widths are different during the mining process of the working face.

Variations in mining height also lead to differences in the distribution characteristics of stress fields in the protective coal pillars of the working face, affecting the migration of leaked methane in gas wells. During coal seam mining, the stress concentration inside the protective pillar primarily appears in the triangular area where the coal wall contacts the roof and floor, and fractures in this area progressively develop and mature. As the 'second open-off cut through' and the working face continues to advance, the stress distribution in the protective pillar evolves from a "parabolic" to a "saddle" shape. Concurrently, as the height of the protective pillar increases, the vertical stress peak of the roof and floor in front of the coal also varies (Figure 4b).

Figure 5 shows that as mining progresses on the working face, stress on the left side of the coal pillar gradually increases until mining is completed, reaching the first peak stress at the protective coal pillar. The peak stresses for different widths of coal pillars are 26.48 MPa, 24.71 MPa, and 24.09 MPa, respectively. After the model reaches equilibrium,

mining the right working face causes stress changes on the right side of the coal pillar. The peak values of the second stress on the right side of the pillar with different widths are 24.05 MPa, 22.76 MPa, and 22.31 MPa, respectively. Comparing the stress peaks reveals that the left side of the coal pillar has higher stress than the right. The stress distribution shows that the influence range of secondary mining is smaller than that of primary mining. For coal pillars of different widths, the range of the smoothed area is 30, 60, and 80 m (Figure 4). The larger the smooth area, the greater the protolith stress or elastic region within the coal pillar. This area has less stress on the coal pillar, and the oil well located here has higher stability. In addition, the stress on the roof sandstone is greatly affected, and the roof is prone to slip and failure. At this time, the protected area of the gas well is relatively small and prone to instability. When comparing the two coal pillar sizes of 180 m and 150 m, it is evident that the 180 m protective coal pillar provides a greater smoothing area, characterized by a smooth zone of 80 m, as illustrated in the accompanying diagram, with minimal differences in stress impact range and vertical stress peak value. The impact of mining around gas wells is smaller, resulting in fewer fractures and easier protection of wells. However, the increase in coal pillar width also means the waste of coal resources.

According to Figure 5, as the coal pillar width increases, the smooth areas between the first and second peak stress also increase, indicating that the elastic areas of the coal pillar gradually increase. At the same time, the peak vertical stress also decreases accordingly. After the completion of mining, compared to the width of the 130 m protective coal pillar, the first stress peak of the 150 m protective coal pillar width decreased by 6.7%, and the second stress peak decreased by 5.3%; the first peak stress of the 180 m pillar width decreased by 9%, and the second stress peak decreased by 7.2%. Through data comparison and analysis, the wider the protective coal pillar, the lower the peak stress. However, when the width of the pillar reaches 150 m and 180 m, the stress peaks are 24.71 MPa and 24.09 MPa, respectively, with a difference of 0.62 MPa—the peak stress and stress diffusion area tend to be similar. Therefore, in practical engineering, the width of the protective coal pillar can be slightly reduced to increase coal production. However, a too-small coal pillar width may threaten the safety of oil/gas wells. When choosing to protect the coal pillar width, it is necessary to consider factors such as coal resource utilization and the safety of oil/gas wells comprehensively.

As illustrated in Figure 6, during the mining process, the stress on the left side of the coal pillar experiences a gradual increase, ultimately reaching the first stress peak. The peak values corresponding to different heights of coal pillars are 27.37 MPa, 28.93 MPa, and 30.73 MPa. Subsequently, upon executing the second open-off cut, the stress distribution on the right side of the coal pillar changes; the peak values of the second stress on the right side of the pillar with different heights are 24.05 MPa, 22.76 MPa and 22.31 MPa. Under identical mining conditions, The higher the protective coal pillar, the greater the peak bearing pressure in front of it (Figures 6 and 7). This is because as the height increases, the roof's thickness decreases accordingly, and the decompression effect on the movement of the upper rock layer becomes smaller. The peak point of the bearing pressure shifts forward, and the range of influence increases. Under the same working face conditions, the peak vertical stress is directly proportional to the height of the protective coal pillar. When the pillar height is 2 m, the peak stress increases by 5.6% and 5.3%. At the height of 4 m, the peak stress rises by 12.2% and 11.2%. As the height increases, the distance between the two vertical stress peaks in the coal pillar shortens, indicating that taller mining heights make oil/gas wells more susceptible to destabilization and damage., and the leaked methane will quickly migrate to the working face. Therefore, appropriate protective measures should be taken. Within the same pillar width, the second peak vertical stress is lower than the first, indicating that the vertical stress borne by the coal pillar on the later mining side is smaller, and the range of stress influence is also smaller.

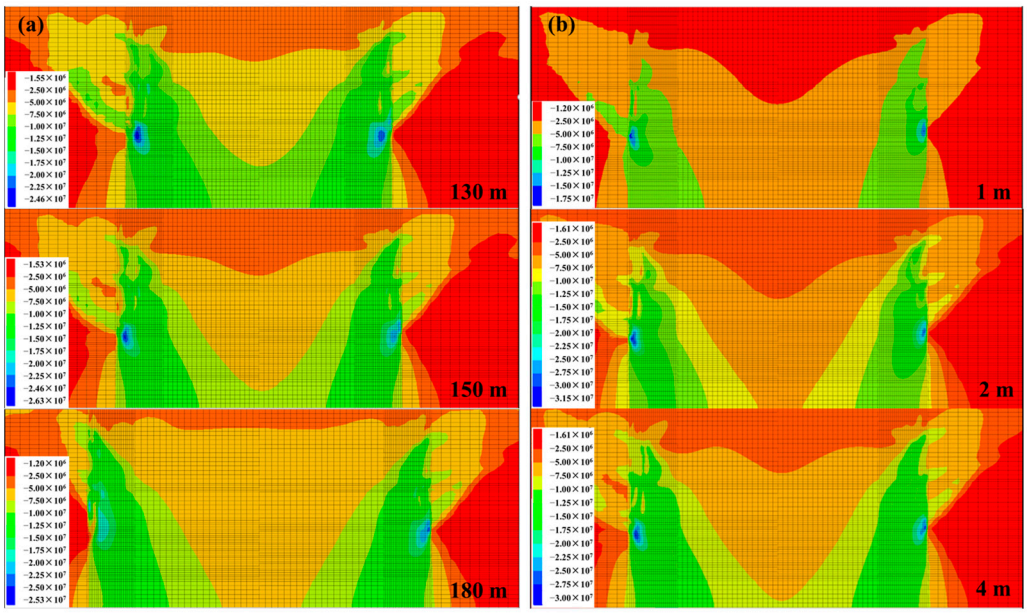


Figure 4. Cloud diagram of vertical stress distribution within protective coal pillars of gas wells of different dimensions ((**a**) different widths and (**b**) different heights).

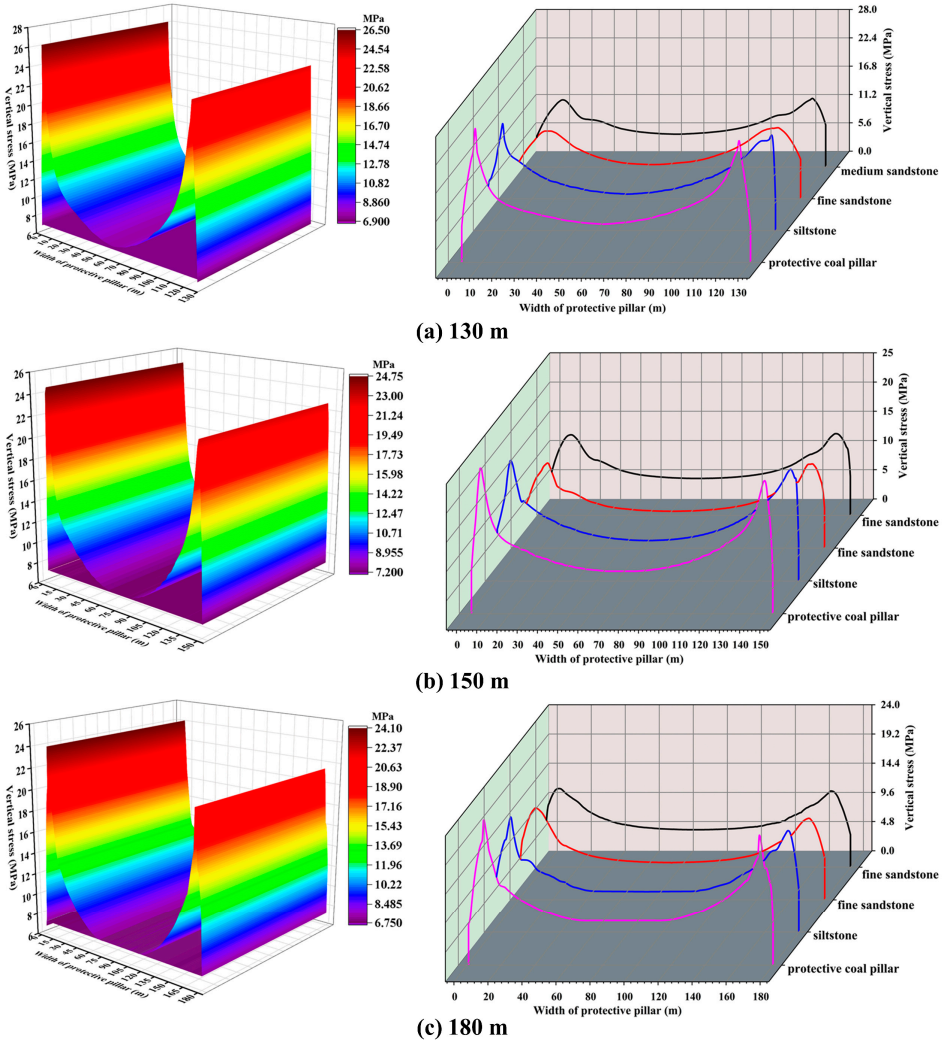


Figure 5. Vertical stress distribution in each rock layer of the protective coal pillar is achieved by gas wells of different widths.

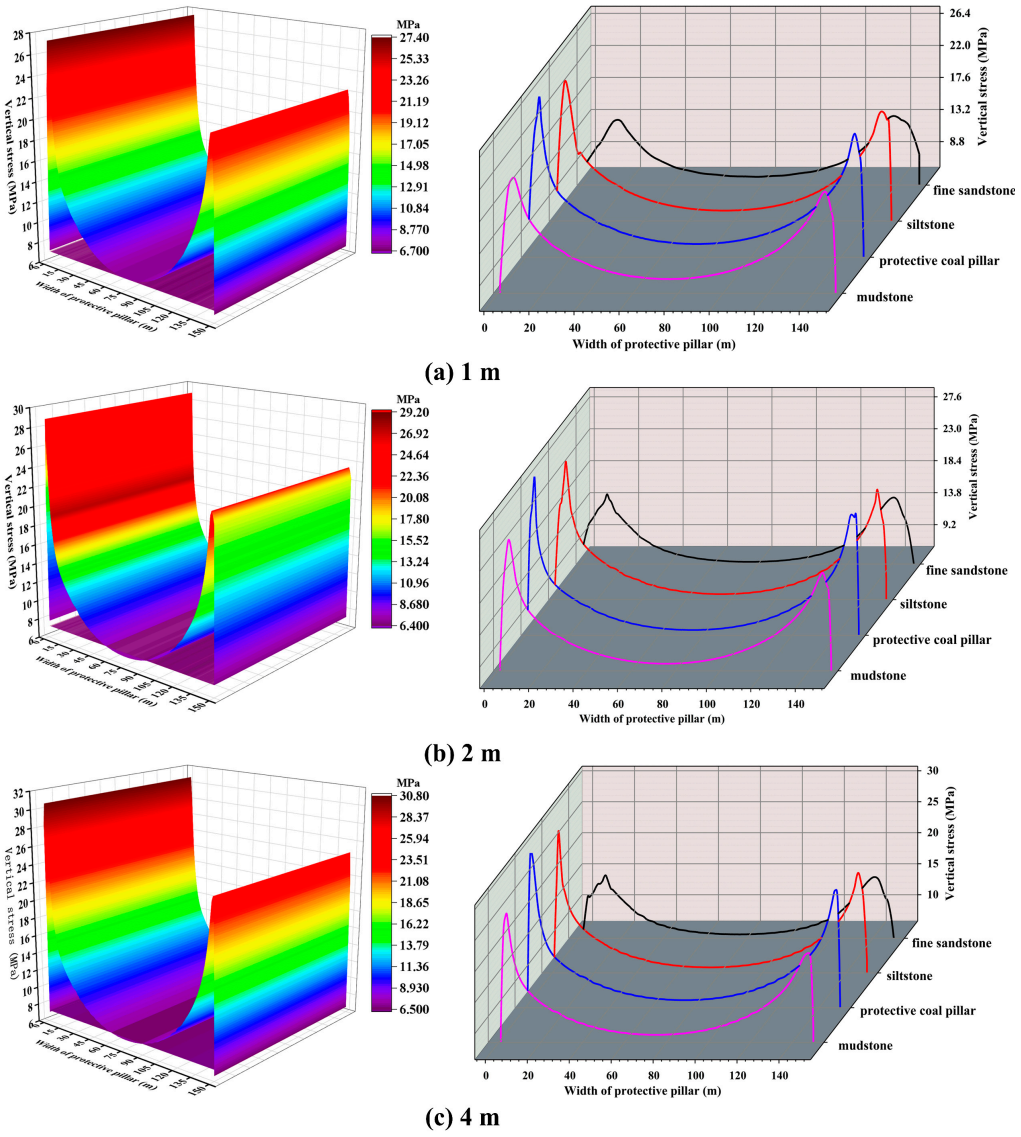


Figure 6. Vertical stress distribution in each rock layer of protective coal pillar by gas wells with different heights.

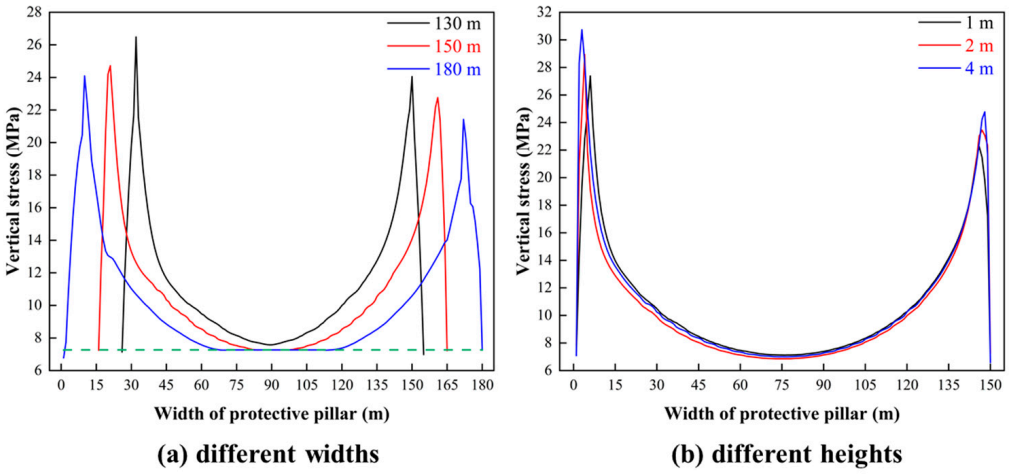


Figure 7. Vertical stress distribution line diagram inside the protective coal pillar of gas wells with different widths and heights.

3. Fracture Scale Division of Mining Disturbed Coal Mass and Control Equation of Methane Migration

During the mining process of the working face, the temporal and spatial evolution of the overburden fractures in the oil/gas wells protective pillars also occurs, resulting in changes in the internal structure of the coal seam and the formation of different scale fractures. The migration behavior of methane in different scale fractures of the coal mass is different, so the methane migration law in the mining fracture field of the coal mass in front of the working face is also changing. In view of this, this study first divides the fracture scale based on the Reynolds number of methane flow states at different fracture scales, establishes the relationship between permeability and each fracture scale, and then constructs the corresponding methane migration behavior control equations for each zone, thereby establishing a complete multi-scale fracture coal mass transport equation in the mining space.

The following assumptions were made for the equations based on coal stress field and methane migration characteristics [22].

(1) Coal is an anisotropic continuous porous medium with dual pores and a single permeability elastic continuous heterogeneous medium. The thermal expansion strain caused by temperature and gas adsorption was ignored in the study;
(2) The leaked methane is considered an ideal gas;
(3) Methane adsorption and desorption rates are very fast and negligible in the process of coal seam methane extraction;
(4) The process of diffusion of leaked methane conforms to Fick's law and is transported as seepage in the fracture;
(5) Methane migration processes are treated as isothermal processes.

3.1. Fracture Scale Classification of Mining Disturbed Coal Mass

According to the transport state of methane, multi-scale fractures within coal pillars can be divided into large-, medium-, and small-scale fractures. Multi-scale fracture classification needs to consider flow velocity and permeability and cannot be limited to scale fracture classification alone. Therefore, in this study, the Reynolds number of different fluid flow regimes combined with permeability are used to classify the scale of fracture.

According to Karman's criterion, the Reynolds number magnitude determines the fluid flow state. Therefore, this study uses the Reynolds number to quantify fracture size and identify the type of methane channel. The Reynolds criterion expression is:

$$\mathrm{Re} = \frac{\rho u r}{\mu} \tag{1}$$

where ρ is the density, u is the flow velocity, d is the diameter of the flow tube, and μ is the dynamic viscosity coefficient.

When the fluid flow state is laminar, its flow conforms to Darcy's law:

$$u = -\frac{k}{\mu}\nabla p \tag{2}$$

where u is the velocity of gas flow in the coal seam, m/s; ∇p is the fluid pressure gradient.

When the fluid flow state is turbulent, the power law can express the fluid velocity:

$$u = -\frac{k}{\mu}\left(\frac{\mathrm{d}p}{\mathrm{d}x}\right)^{s} \tag{3}$$

Relating the Reynolds number equation to the fracture of the methane channel, it can be obtained:

$$r = \mathrm{Re}\frac{\mu}{\rho u} \tag{4}$$

where r is the fracture scale. When the Reynolds number is less than 2320, the flow state of methane is linear laminar flow; when the Reynolds number is between 2320 and 4000, the flow state of methane is transitional flow; and when the Reynolds number is more than 4000, the flow state of methane is turbulent flow, which can be obtained by association of Equations (1)–(4) and Re the range of values:

Classified as small scale when the fracture width is $r \le \frac{2320\mu^2}{\rho k} / \frac{dp}{dx}$, medium scale when the fracture width is $\frac{2320\mu^2}{\rho k} / \left(\frac{dp}{dx}\right)^s < r < \frac{4000\mu^2}{\rho k} / \left(\frac{dp}{dx}\right)^s$, and large scale when the fracture width is $r \ge \frac{4000\mu^2}{\rho k} / \left(\frac{dp}{dx}\right)^s$.

3.2. Control Equation for Methane Migration in the Mining-Disturbed Coal Mass

3.2.1. Governing Equations of Methane Migration Behavior in Mesoscale and Small-Scale Fractures

Regarding the flow of methane in medium scale (roof and floor fracture zones, advanced plastic coal mining fractures in the working face) and small-scale fractures within the mined coal rock mass. Essentially, it is an unstable gas flow process in the mining-induced stress field environment.

The tensor expression of the stress balance equation for an elastic porous medium system is:

$$\sigma_{ij,j} + f_i = 0 \tag{5}$$

where σ_{ij} is the component of the stress tensor and f_i is the volume force component.

The strain–displacement relationship is expressed as ε_{ij}, $u_{i,j}$ is the displacement component.

$$\varepsilon_{ij} = \frac{1}{2}\left(u_{i,j} + u_{j,i}\right) \tag{6}$$

In this study, it is assumed that the coal mass is an ideal elastic body, therefore, can be expressed by the generalized Hooke's law:

$$\varepsilon_{ij} = \frac{1}{2G}\sigma_{ij} - \left(\frac{1}{6G} - \frac{1}{9K}\right)\sigma_{kk}\delta_{ij} + \frac{\alpha_m p_m + \alpha_f p_f}{3K}\delta_{ij} + \frac{\varepsilon_s}{3}\delta_{ij} \tag{7}$$

where $G = E/2(1+v)$, $K = E/3(1-2v)$, $\alpha_m = 1 - K/Ks$, $\alpha_f = 1 - K(LmKn)$, $Ks = Es/3(1-2v)$, $\sigma_{kk} = \sigma_{11} + \sigma_{22} + \sigma_{33}$, $\varepsilon_s = \varepsilon_l p_m/(P_L + p_m)$, where G is the shear modulus of the coal, K is the bulk modulus of the coal, Ks is the elastic modulus of the coal skeleton, E is the elastic modulus of the coal, v is the Poisson's ratio of the coal, Kn is the fracture stiffness, Lm is the width of the matrix, δ_{ij} is the Kronecker's factor, α_m and α_f are the effective stress coefficients of the coal matrix and the fracture of the coal, p_m and p_f are the pressure of the matrix and the fracture pressure of the coal, ε_s is the volume strain of the matrix caused by gas adsorption/desorption, ε_l is the Langmuir-type strain coefficient, and P_L is the Langmuir pressure constant.

Associative Equations (5)–(7) can be obtained to control the stress field during the methane process in the coal seam:

$$Gu_{i,jj} + \frac{G}{1-2v}u_{j,ji} - \alpha_p p_{f,i} - K\varepsilon_{s,i} + f_i = 0 \tag{8}$$

In this paper, methane is treated as an ideal gas to simplify the calculation and research process. The ideal gas model can adequately explain the movement and transportation laws

of methane within coal seams, and it also serves as a valuable reference for studying the pore structure and permeability characteristics of methane in coal-rock masses. By adhering to the ideal gas state equation, a more accurate description of the state and properties of methane in coal seams can be obtained.

$$pV = \frac{m}{M} R_0 T \tag{9}$$

The relationship between methane pressure and methane gas density can be derived as

$$\rho_g = \eta p \tag{10}$$

$$\eta = \frac{M}{\mathrm{R}T} \tag{11}$$

Where T is the absolute temperature; R is the universal coefficient, M is the Mohr mass of the gas, kg/mol, and ρ_g is the density of methane at a methane pressure of p.

Methane in the coal seam has two states: adsorbed methane on the surface of coal rock pores and free methane in the form of free flow in fracture spaces. The content of free methane can be expressed as Q_1 [23], kg/m^3.

$$Q_1 = \eta p \phi \tag{12}$$

The formula for the adsorbed methane content per unit volume of coal surface can be obtained based on the Langmuir adsorption analytical equation [24]:

$$Q_2 = \frac{abp}{1 + bp} \rho_0 \rho_c \tag{13}$$

Q_2 is the adsorbed methane content, kg/m^3, a, b are adsorption constants, p is the adsorption equilibrium methane pressure, MPa, A is the ash content of coal, %, T_0 is the experimental temperature when the adsorption constants of coal were determined, W is the moisture of the coal seam, %, and the methane content can be expressed as:

$$Q = Q_1 + Q_2 = \eta p \phi + \frac{abp}{1 + bp} \rho_0 \rho_c \tag{14}$$

Conservation of mass in microunits in coal seams is obtained by considering the mass source term:

$$\nabla (\rho_g u) + \frac{\partial (Q)}{\partial t} = Q_m \tag{15}$$

Q is the methane content of the coal seam per unit volume of the coal seam, kg/m^3; u is the methane flow rate, m/s; ρ_g is the density at methane pressure P, kg/m^3; and Q_m is the mass source term, kg/m^3.

For small and medium-scale fracture, the association of Darcy's law and the continuity equation for methane yields.

$$\nabla (\rho_g u) + \frac{\partial (Q)}{\partial t} = Q_m \tag{16}$$

Combined with the methane equation of state $\rho_g = \eta p$, taking the mass source term $Q_m = 0$, the mathematical model of methane flow can be found.

$$\left(\frac{ab\rho_0 \rho_c}{(1 + bp)^2} + \eta \phi \right) \frac{\partial p}{\partial t} + \eta p \frac{\partial \phi}{\partial t} - \nabla \left(\eta p \frac{k}{\mu} \frac{dp}{dx} \right) = 0 \tag{17}$$

Based on the theoretical model of matchstick permeability and the Kozeny-Carman equation, the permeability can be expressed as [25]

$$k = k_0 e^{-3c_f(\sigma_b - \sigma_{b0})} \tag{18}$$

where k is the permeability of coal mass, mD; ϕ is the fracture porosity; and c is the KC constant. Unfractured coal typically has a permeability in the range of 0.1 to 10 millidarcies (mD), while fractured coal can have permeabilities ranging from 10 to 1000 mD or more, depending on the extent and connectivity of the fractures.

The cubic law can obtain the single fracture flow rate of gas in coal mass as:

$$q = -\frac{r^3}{12\mu}\frac{\Delta p}{L} \tag{19}$$

where r is the width of coal fracture, m; μ is the dynamic viscosity of methane gas, Pa·s; Δp is the pressure difference of coal fracture, Pa; L is the length of coal fracture, m.

Coal seam methane is produced per unit of time:

$$q = S\frac{k}{\mu}\frac{\Delta p}{L} \tag{20}$$

where S is the cross-sectional area, according to the unit volume porosity $\varphi = bS$, denote the variation of coal porosity with effective stress by Λ, $\Lambda = \frac{1}{\varphi}\frac{\partial \varphi}{\partial \sigma'}$. The above equation can be rewritten as:

$$\frac{\partial k}{\partial \sigma'} = 3\Lambda k \tag{21}$$

The damage variable is invoked to define the fracture development and permeability changes within the coal mass under mining-induced stress, and the damage variable can be expressed in terms of the elastic modulus as [26]:

$$\frac{E}{E_0} = 1 - D \tag{22}$$

where E_0 is the modulus of elasticity of the elastic phase of the coal.

Λ can be represented by the damage variable D, γ which is the sensitivity impact factor.

$$\Lambda = \gamma D \tag{23}$$

Equation (22) can be written as:

$$\frac{\partial k}{\partial \sigma'} = 3\gamma D k \tag{24}$$

Below is the permeability modeling of the mesoscale fracture:

$$k = k_0 e^{3\gamma D(\sigma' - \sigma_0')} \tag{25}$$

3.2.2. Governing Equations for Methane Migration Behavior in Large-Scale Fracture

In the goaf, cavities are formed after coal seam mining, which are filled with gangue and air. There are a large number of cavities and fractures between these gangues, and the gas flow state is between Darcy seepage and Navier–Stokes pipeline flow. To describe the rapid flow of fluids in this porous medium, the Brinkman equation can be used:

$$-\nabla \cdot \frac{\eta}{\varphi}\left(\nabla \boldsymbol{u}_{\mathrm{br}} + (\nabla \boldsymbol{u}_{\mathrm{br}})^{\mathrm{T}}\right) - \left(\frac{\eta}{\varphi}\boldsymbol{u}_{\mathrm{br}} + \nabla p_{\mathrm{br}}\right) = 0 \tag{26}$$

where φ is the porosity; k is the permeability coefficient.

Since the roadways and working face ventilation can be considered pipe flow, the Navier–Stokes equations can describe the flow of gases in them.

$$-\nabla \cdot \eta\left(\nabla \boldsymbol{u}_{\mathrm{ns}} + (\nabla \boldsymbol{u}_{\mathrm{ns}})^{\mathrm{T}}\right) + \rho \boldsymbol{u}_{\mathrm{ns}} \cdot \nabla \boldsymbol{u}_{\mathrm{ns}} + \nabla p_{\mathrm{ns}} = 0 \tag{27}$$

$$\nabla \cdot \boldsymbol{u}_{\mathrm{ns}} = 0 \tag{28}$$

where η is the coefficient of viscosity and $\boldsymbol{u}$ is the velocity vector.

Methane migration obeys the hydrodynamic dispersion law due to the stochastic nature of the movement of methane molecules in the fluid. The study of convection–diffusion equations in porous media allows for a better understanding of the methane migration laws in mining:

$$\theta_s \frac{\partial c}{\partial t} + \nabla \cdot (-\theta_s D_L \nabla c + uc) = S_c \tag{29}$$

where θ_s is the volume of fluid per unit area per unit time,S_c is a measure of the mass of a substance transferred by diffusion per unit area over a unit time, c is the dissolved concentration, and D_L is the permeability tensor.

Before methane diffusion reaches equilibrium, the diffusion equation for the concentration of substance c with time t and position r is:

$$\frac{\partial c}{\partial t} = D\left(\frac{\partial^2 c}{\partial r^2} + \frac{2}{r}\frac{\partial c}{\partial r}\right) \tag{30}$$

A combination of these equations can be used to study the methane migration pattern in the goaf medium more accurately.

4. The Migration Law of Leaked Methane Within the Gas Well Protective Coal Pillar Under the Influence of Mining

Coal pillars are affected by stress during coal mining, resulting in varying degrees of damage within the coal mass and forming fractures of different scales. This increases the permeability of the coal mass by several orders of magnitude. There are significant differences in the migration behavior of methane within fractured coal masses at different scales. This chapter studies the influence of different factors on the migration and permeability evolution of leaked methane in coal pillars under the influence of mining, based on mathematical models of methane migration in fractures of different scales and taking Shuangma Coal Mine as the background.

4.1. Establishment of Numerical Model

An abandoned gas well in the working face is near the center of the working face (Figure 8), and this study simulates the gas pressure of 15 MPa for the oil and gas well. COMSOL Multiphysics was used to study the methane migration law of the gas wells in the coal pillar. A large amount of research has been conducted in the early stage to validate this model, and it has been confirmed that the model established in this paper is effective in simulating the entire process of methane seepage in coal seams [10] In order to better simulate the onsite work, this simulation models the overall range of the coal pillar. Model assignment parameters refer to previous research. The specific parameters are shown in Table 2 [27,28].

The model considers the length of the working face at the site, the location of the abandoned gas wells, and the extent and dimension of the protective coal pillar. A free tetrahedral mesh was applied, and three kinds of rectangular protective coal pillars of 130 × 130 × 4 m, 150 × 150 × 4 m and 180 × 180 × 4 m were constructed. The gas well,

with a radius of 0.15 m, is situated at the center of the coal pillar. The radius of the gas well is consistent with that onsite, as shown in Figure 9.

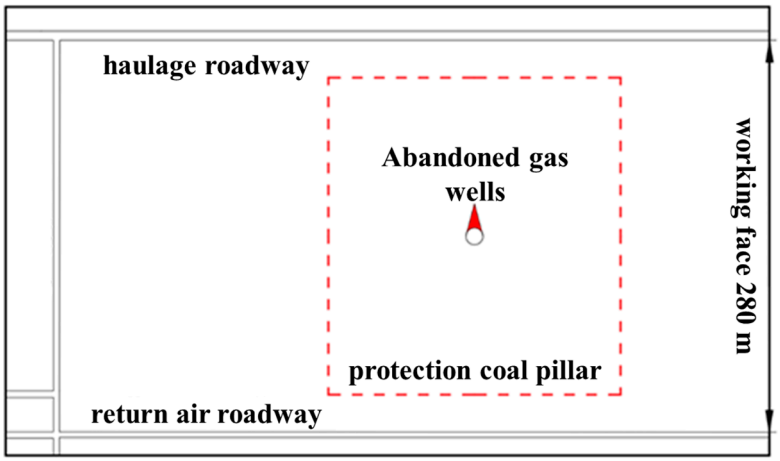


Figure 8. Location of the abandoned gas wells and range of protective coal pillars in Shuangma coal mine.

Table 2. COMSOL assignment parameters.

Parameter	Numerical Value	Parameter	Numerical Value
Initial fracture methane pressure, pfg0	0.1 [MPa]	Well pressure, pc	15 [MPa]
Langmuir volume parameters, VL	0.072 m^3/kg	Capillary weight of overburden, ρ_r	2550 kg/m^3
Langmuir pressure constant, P_L	3.034 MPa	Fracture stiffness, Kn	4.8 [GPa]
Coal Skeleton Density, ρ_c	1400 kg/m^3	Initial fracture porosity, φ_{f0}	0.021
Poisson's ratio of a coal, ν	0.3	Initial matrix porosity, φ_{m0}	0.045

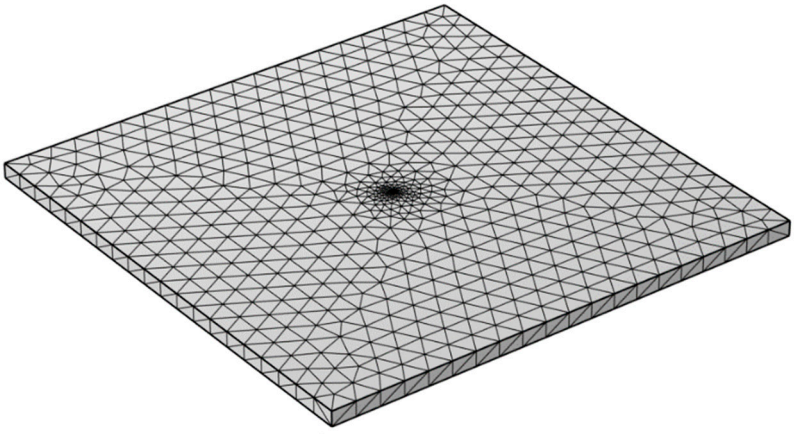


Figure 9. Model construction and meshing in COMSOL Multiphysics 6.2 (COMSOL Co., Ltd, Shanghai, China).

4.2. The Migration Law of Leaked Methane Within Protective Coal Pillars with Different Widths

When the protective coal pillar is 130 m wide, the diffusion time of leaked methane is within 0–80 days; during this period, methane has not yet diffused to the sides, resulting in higher pore pressure within the coal pillar and lower coal permeability. As the diffusion time reaches 100 days, the permeability of leaked methane in the pillar has reached equilibrium; between 100 and 120 days, external stress on both sides of the coal pillar increases, leading to a rise in pore pressure compared to levels before 80 days with permeability also increasing and reaching equilibrium. At this point, permeability on the sides of the pillar is higher than around the gas wells (Figure 10).

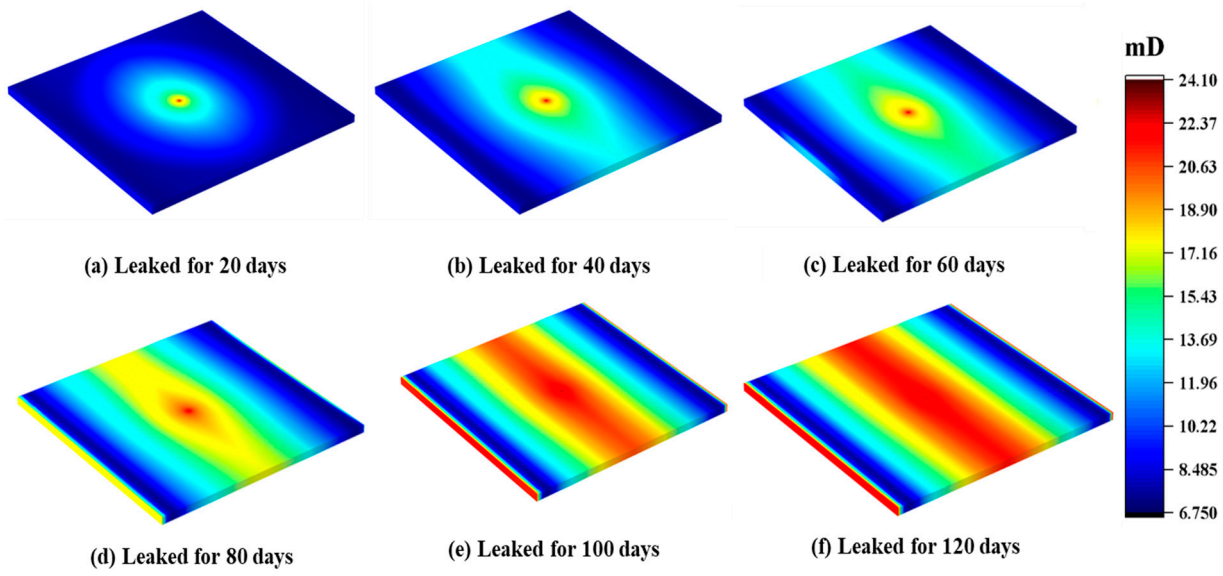


Figure 10. Spatiotemporal evolution cloud diagram of permeability of protective coal pillar with a width of 130 m.

The closer the protective coal pillar is to the oil/gas well, the greater the permeability change. However, in small- and medium-scale transition areas, the permeability change remains minimal as these areas maintain equilibrium for a long time. When the width of the pillar increases to 150 m and 180 m (Figures 11 and 12), the overall permeability evolution in the pillar is similar to that of the 130 m width. However, due to the wider width of the protective coal pillar and the wider elastic zone, it is more difficult for leaked methane to diffuse into mesoscale fractures. Therefore, when the width of the pillar is 150 m, the leaked methane reaches equilibrium within 160 days of diffusion, and when the width of the pillar is 180 m, the leaked methane reaches equilibrium within 180 days. As the width of the pillar increases, the permeability of leaked methane also increases. This is because the width of the protective coal pillar is different, and the external stress on both sides is different, resulting in a small difference in pore pressure and effective stress, leading to different permeability.

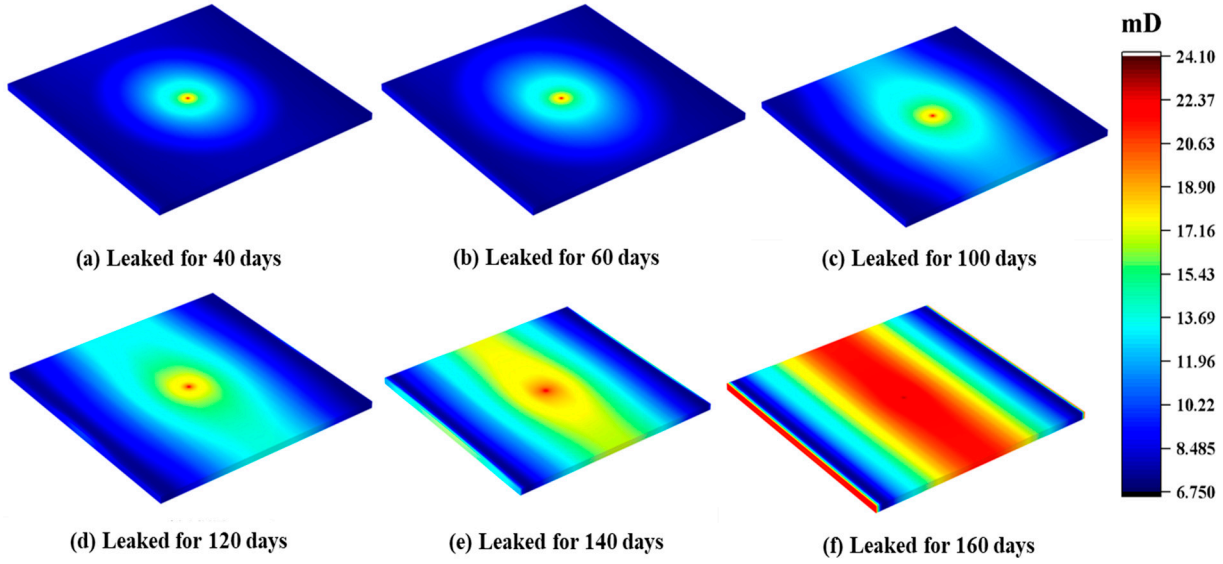


Figure 11. Spatiotemporal evolution cloud diagram of permeability of protective coal pillar with a width of 150 m.

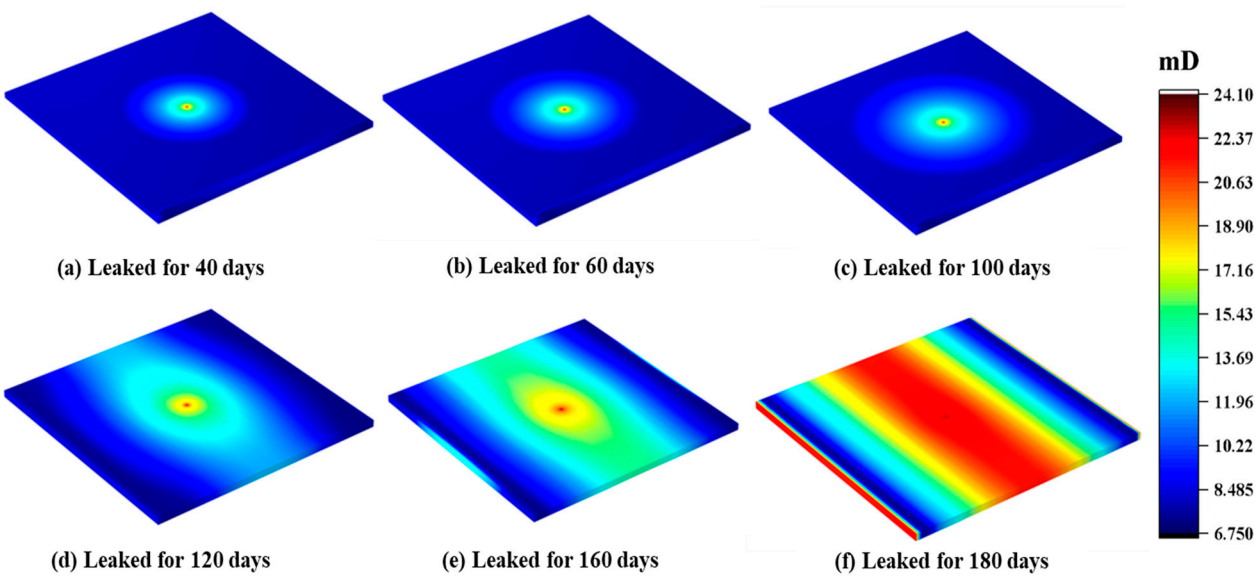


Figure 12. Spatiotemporal evolution cloud diagram of permeability of protective coal pillar with a width of 180 m.

The permeability evolution curve within the pillar exhibits a "W" shape (Figure 13). When the width of the protective coal pillar is 130 m, the permeability increases by 1.87 mD, 5.78 mD, and 10.52 mD at different time intervals during leaked methane from 0 to 80 days. When the methane leakage reaches 100 days, the permeability of the coal on both sides of the pillar slowly increases with the increase of leaked days, with the permeability increasing by 18.25 mD and 22.91 mD, respectively. This is because the leaked methane has reached equilibrium at this time, and the difference in pore pressure changes is small. With the increase of time, the difference between the permeability on both sides of the pillar and the permeability in the transition zone of small and medium scales also increases. At this point, a complete methane migration channel has been formed inside the pillar; At 120 days of leaked methane, the permeability on the left side of the pillar was 22.91 mD, and the permeability on the right side was 21.79 mD. The difference in peak permeability on both sides was due to the different external mining-induced stresses experienced. By studying the evolution law of permeability within the pillar, it can be concluded that under the influence of mining, the mesoscale fractures formed on both sides of the pillar due to the influence of mining-induced stress will lead to a sudden increase in the permeability of transition zone. The permeability is inversely proportional to the magnitude of mining-induced stress, which is mainly dominated by mining-induced stress.

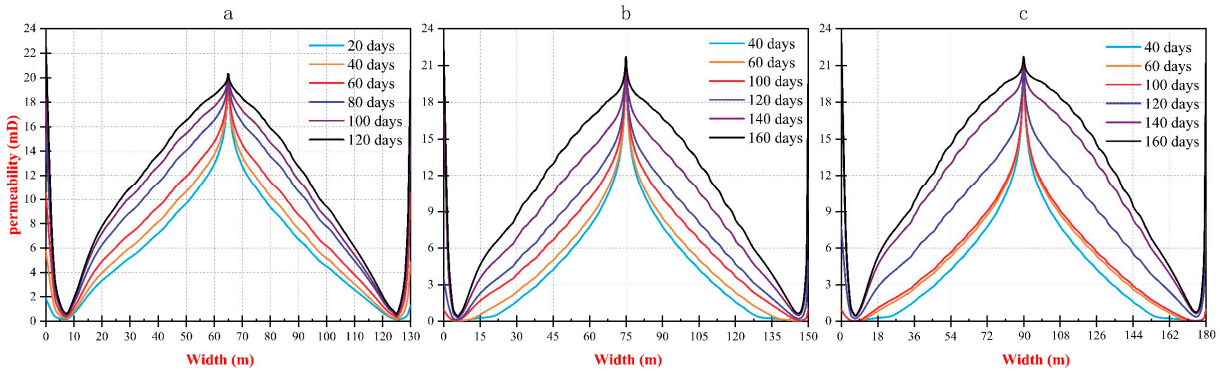


Figure 13. Line plots of the spatial and temporal evolution of permeability of protective coal pillars of different widths ((**a**) 130 m, (**b**) 150 m, and (**c**) 180 m).

From the transition zone to the surrounding area of the gas well, the evolution of permeability is mainly dominated by pore pressure. At this time, the leaked methane channel is a small-scale fracture, and the change in permeability is relatively small compared to the mesoscale. The maximum permeability around the gas well is mainly due to the high pore pressure. The speed at which coal is extracted can lead to different stress distributions within the coal seam and the surrounding strata. Faster exploitation rates can result in more rapid stress changes, potentially leading to earlier and more extensive fracturing. This increased fracturing can create additional pathways for methane to migrate, thus affecting the overall permeability of the coal mass. This can accelerate the migration of methane from the coal seam into the mining area, posing a greater risk of methane accumulation and potential gas outbreaks. In the initial stages of leakage, pore pressure around the gas wells is high, and the effective stress is low, resulting in maximum permeability. However, as leaked days increase, permeability on both sides of the pillar gradually rises. Due to continuous pressurization of the gas wells, leaked methane diffuses and transports through fractures of various scales. Ultimately, permeability on both sides of the pillar exceeds that around the gas wells. The increase in permeability near the working faces on both sides of the pillar indicates that the stress on both sides is smaller, and larger mesoscale fractures are generated, making it easier for leaked methane to diffuse. In addition, the permeability inside the pillar increases with the increase of the pillar width. After balancing, the peak permeability on both sides of the pillar is smaller when the pillar width is 130 m compared to 150 m and 180 m. This is the result of different mining-induced stresses. When the pillar widths are 150 m and 180 m, the permeability difference on both sides of the pillar is only 1 mD, indicating that these two widths achieve a similar effect.

4.3. The Migration Law of Leaked Methane from Protective Coal Pillars with Different Heights

Figures 14–16 show that as mining height increases, permeability on both sides of the protective coal pillars and around the gas wells decreases. This is because increased mining height results in higher mining-induced stress and lower effective stress, leading to reduced permeability. When the leakage days are 120 days, the permeability distribution in the 1 m-high pillar becomes stable and no longer changes. However, the permeability within pillar heights of 2 m and 4 m is still evolving, and the permeability on both sides of the pillar changes accordingly. This is mainly due to the high stress applied, which leads to slow diffusion of leaked methane.

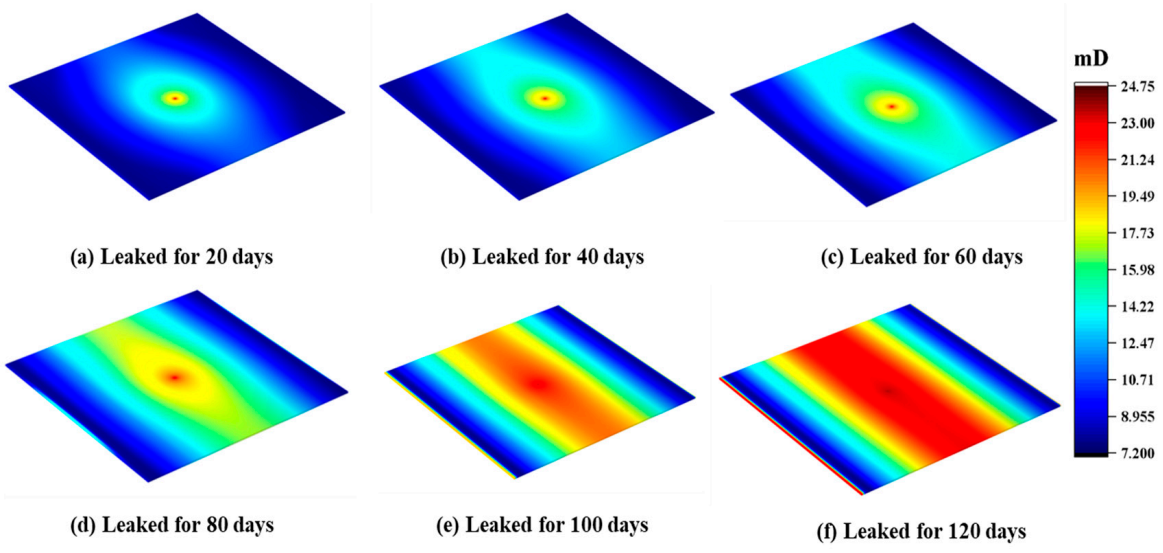


Figure 14. Spatiotemporal evolution cloud diagram of permeability at 1 m height of protective coal pillar.

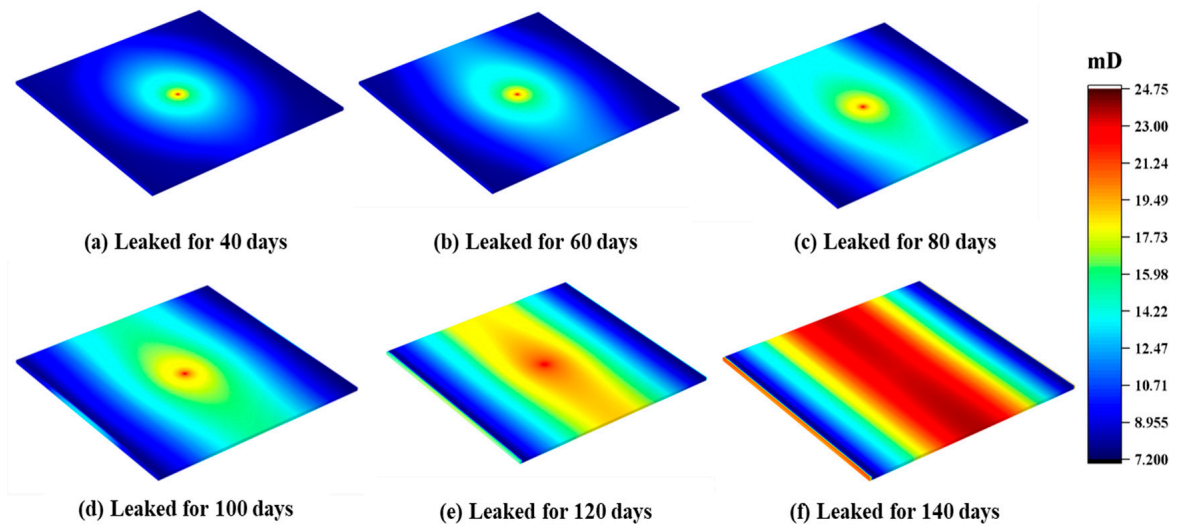


Figure 15. Spatiotemporal evolution cloud diagram of permeability at 2 m height of the protective coal pillar.

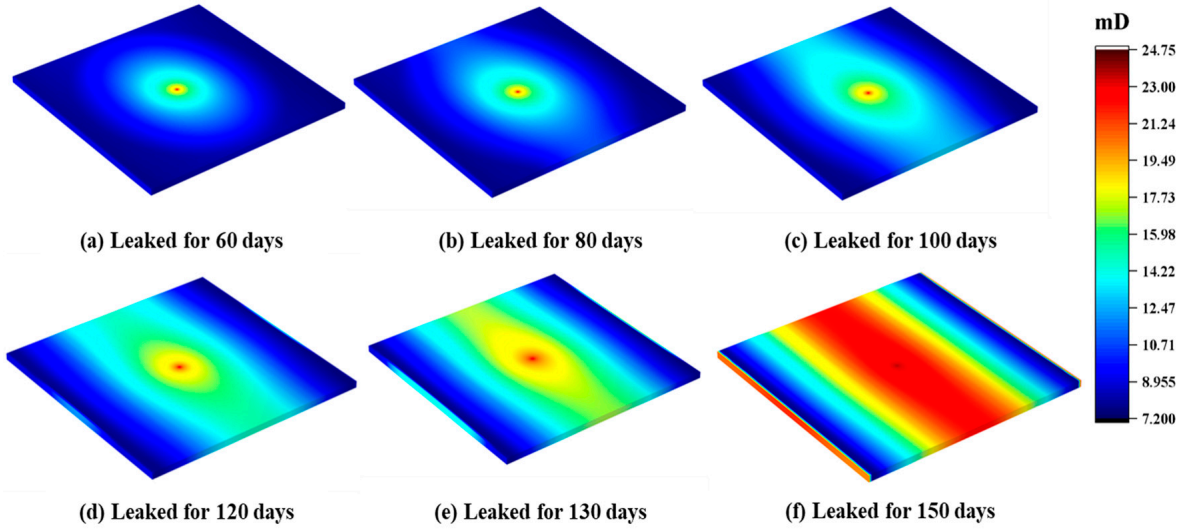


Figure 16. Spatiotemporal evolution cloud diagram of permeability at 4 m height of the protective coal pillar.

The overall permeability within the protective coal pillar at varying heights shows a trend of decreasing, increasing, then decreasing, and increasing again (Figure 17). This is because, under the influence of mining, both sides of the pillar are subjected to significant stress, leading to damage and plastic deformation of the coal mass, resulting in mesoscale fracture. When the supporting pressure decreases, the area between the plastic and elastic zones of the coal pillar is affected by stress, and fractures begin to close, resulting in lower permeability. After fully entering the elastic zone, the permeability is mainly affected by the stress around the gas well, resulting in high pore pressure and a further increase in permeability.

For instance, when the coal pillar height is 1 m and leaked methane reaches 120 days, a complete methane migration channel forms within the pillar. During this time, permeability on the left side drops sharply from 20.03 mD to 0.42 mD, which is a mesoscale fracture development stage. Afterward, the permeability around the gas well slowly increased, and the transition zone between small and medium scales slowly decreased, finally rising sharply to 22.02 mD. The different permeability on both sides of the pillar is caused by different peak stress.

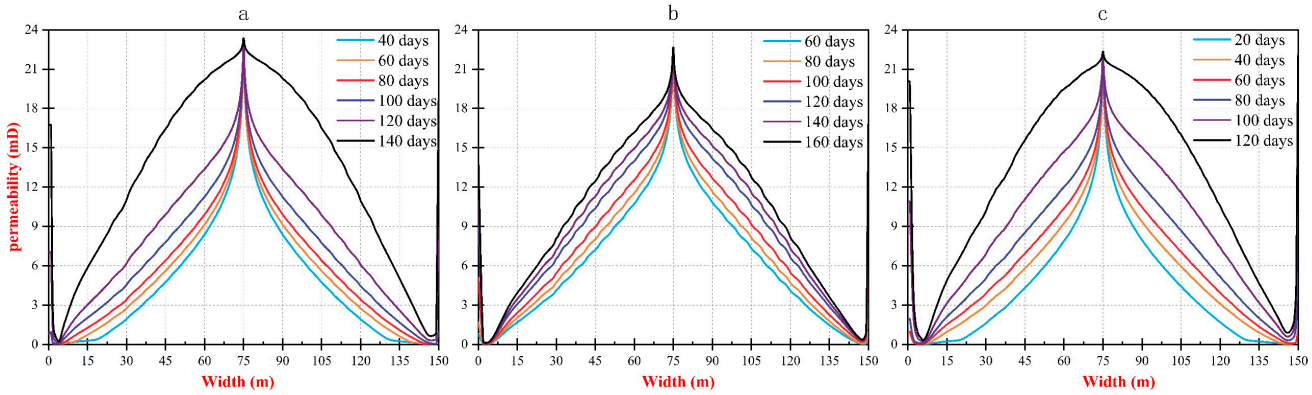


Figure 17. Line plots of the spatial and temporal evolution of permeability of protective coal pillars at different heights ((**a**) 1 m, (**b**) 2 m, and (**c**) 4 m).

Within protective coal pillars of varying heights, permeability trends are primarily influenced by mining-induced stress and the pressure from gas wells, while the magnitude of permeability values is mainly driven by mining-induced stress. As the pillar's height increases, the mining height and mining-induced stress also increase, expanding the damaged area. At this stage, the combined effects of mining-induced stress and gas well pressure lead to a decrease in permeability. When small-scale fracture transitions into medium-scale fracture, permeability values increase rapidly.

5. Discussion

This study is based on the background of the remaining oil/gas well-protective pillars in the Shuangma Coal Mine. The evolution characteristics and spatial distribution of mining-induced stress fields in pillars of different widths and heights were studied through numerical simulation. It was found that the stress inside the protective coal pillars of different sizes was asymmetrically distributed in a 'saddle' shape. As the pillar's height increased, the peak vertical stress of the roof and floor in front of the rib also increased. The higher the height, the greater the range of the caving zone and the height of fractured zone development, laying the foundation for subsequent research on the diffusion law of methane in the protective coal pillar. Similar patterns were observed by Manoj Khanal [29] and Manchao He [30] in their analyses of deep mining dynamics, mining-induced overburden deformation, and associated stress redistribution (Figure 18), validating the accuracy of the conclusions in this study.

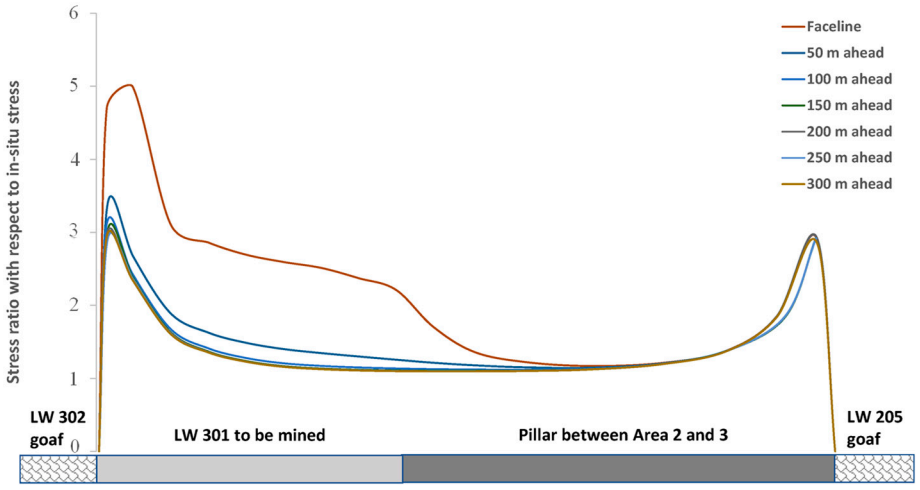


Figure 18. Vertical stress development ahead of longwall 301 [29].

Previous studies on the design of oil/gas wells protective pillar dimensions have primarily focused on intact wells with no leakage of toxic or harmful gases [3,11,12]. This study explores the evolution of stress and methane migration in protective coal pillars for oil/gas wells; from the perspective of leaked gas diffusion, it provides an idea for remaining coal pillars in under-protected oil/gas wells and abandoned oil/gas wells.

While the research provides valuable insights into the evolution of mining-induced stress and the migration of leaked methane in protective coal pillars for gas wells, it is essential to acknowledge and discuss the limitations of the study. The paper has modeled methane as an ideal gas, which simplifies the mathematical representation of fluid flow within the coal seam. This assumption is valid for many practical purposes, particularly when the pressure and temperature variations are not extreme. However, under conditions of high pressure and low temperature, deviations from ideal gas behavior may occur, which could affect the accuracy of flow predictions. Future studies could incorporate real gas behavior into the model to account for such deviations, especially in regions where the pressure and temperature conditions are known to be outside the ideal gas range.

In this study, simulations are based on specific geological and mining conditions at the Shuangma Coal Mine. The generalization of the findings to other coal mines with different geological structures and mining practices requires caution. Each mining site may have unique characteristics that could influence the stress distribution and methane migration pathways. Therefore, site-specific adjustments and validations may be necessary when applying findings to other locations.

6. Conclusions

(1) The stress of oil/gas well-protective coal pillars of different sizes is asymmetrically distributed in a saddle shape; vertical stress peaks on the initial mining side are higher than those on the later mining side, and the elastic region between these peaks expands with increasing pillar width. As the pillar's height increases, the bearing pressure's peak gradually shifts inward within the pillar, and the range of influence gradually increases. The stress in front of the pillar is more concentrated, and the vertical stress peak of the roof and floor in front of the rib is also increasing. The higher the height, the larger the collapse range of the overburden and the height of the fracture zone development, and the greater the damage to the stability of the oil/gas wells arranged in it.

(2) This study establishes the relationship between three different fracture widths and permeability, forming the methane migration equation for multi-scale fracture. Based on the matchstick theory model, a permeability model suitable for small fractures in the elastic stage was derived. The degree of damage was used to describe the development of fracture, and a permeability model suitable for mesoscale fractures was derived. For large-scale fractures in the goaf, the Brinkman equation was used to describe the rapid fluid flow in the pore medium.

(3) The overall evolution curve of methane permeability leakage in protective coal pillars with different widths and heights shows a "W" shape. In the initial stage of leaked methane migration, the permeability around the oil/gas well is the highest. As the number of leaked days increases, the permeability on both sides of the pillar gradually increases, and ultimately, the permeability on both sides of the pillar is greater than that around the oil/gas well. In addition, the permeability on the left side is greater than on the right side. Within the same period of time, the wider the pillar, the slower the diffusion of leaked methane and the lower the permeability. The permeability around the oil/gas well also decreases, and the pressure of leaked methane gradually

decreases. The slower the diffusion of methane, the higher the mining height, the greater the mining stress, and the lower the permeability.

(4) The simulation results show that when the protective coal pillar widths in the Shuangma Mine are 150 m and 180 m, the stress peak values and the stress smoothing areas are found to be similar, with a stress peak difference of 0.62 MPa and a stress smoothing area difference of 20 m. The permeability difference on both sides of the pillars is only 1 mD, indicating a similar effect for both coal pillar widths. Therefore, the site may consider reducing the coal pillar width to 150 m to increase coal production.

(5) The conclusions drawn in the paper are ideal and based on the geological conditions of the Shuangma Mine. Applying these conclusions to other sites will require site-specific adjustments and validation.

Author Contributions: Conceptualization: J.S., S.L. and Y.H.; methodology: J.S., S.L. and Y.H.; formal analysis and investigation: Z.M., W.H. and J.S.; writing—original draft preparation: J.S. and Y.H.; writing—review and editing: S.L., J.S., X.L. and S.X. funding acquisition: S.L.; supervision: J.S., S.L and C.L. All authors have read and agreed to the published version of the manuscript.

Funding: This work is supported by the National Natural Science Foundation of China (No. 52174139), the Postgraduate Research and Practice Innovation Program of Jiangsu Province (KYCX24_2880), and the Graduate Innovation Program of China University of Mining and Technology (2024WLJCRCZL019).

Data Availability Statement: The original contributions presented in this study are included in the article. Further inquiries can be directed to the corresponding author.

Conflicts of Interest: Author Yisong Hao was employed by Shaqu No. 2 Mine Huajin Coking Corporation Limited. Authors Zhi Ma and Weisheng He were employed by Ningxia Coal Industry Limited Liability Company Shuangma Coal Mine, China Energy Group. Author Xu Liang was employed by Shaanxi Xiaobaodang Mining Corporation Limited. Authors Shaoyou Xu and Changheng Luo were employed by No. 2 Gas Production Plant of Sinopec North China Oil and Gas Company. The remaining authors declare that the research was conducted in the absence of any commercial or financial relationships that could be construed as a potential conflict of interest.

References

1. Hao, D.Y.; Zhang, T.; Yang, Y.B.; Ren, J.M. Study on the disturbance characteristics and control strategies of coordinated exploitation of superimposed resources of coal and oil-type gas in Ordos Basin. *Energy Sci. Eng.* **2023**, *11*, 3964–3978. [CrossRef]
2. Liu, J.; Yang, T.; Wang, L.; Chen, X. Research progress in coal and gas co-mining modes in China. *Energy Sci. Eng.* **2020**, *8*, 3365–3376. [CrossRef]
3. Liang, S.; Han, H.; Elsworth, D.; Fu, X.; Yao, Q.; Kang, J.; Li, X.; Li, X. Evolution of Production and Transport Characteristics of Steeply-Dipping Ultra-Thick Coalbed Methane Reservoirs. *Energies* **2020**, *13*, 5081. [CrossRef]
4. Gianoutsos, N.J.; Haase, K.B.; Birdwell, J.E. Geologic sources and well integrity impact methane emissions from orphaned and abandoned oil and gas wells. *Sci. Total Environ.* **2024**, *912*, 169584. [CrossRef]
5. Wang, X.; Ma, H.; Qi, X.; Gao, K.; Li, S. Study on the Distribution Law of Coal Seam Gas and Hydrogen Sulfide Affected by Abandoned Oil Wells. *Energies* **2022**, *15*, 3373. [CrossRef]
6. Zhang, P.; Dougherty, H.; Su, D.; Trackemas, J.; Tulu, B. Influence of longwall mining on the stability of gas wells in chain pillars. *Int. J. Min. Sci. Technol.* **2020**, *30*, 3–9. [CrossRef]
7. Wang, X.; Zhang, Q.; Yuan, L. A coupled thermal-force-chemical-displacement multi-field model for underground coal gasification based on controlled retraction injection point technology and its thermal analysis. *Energy* **2024**, *293*, 130614. [CrossRef]
8. Raimi, D.; Krupnick, A.J.; Shah, J.; Thompson, A. Decommissioning Orphaned and Abandoned Oil and Gas Wells: New Estimates and Cost Drivers. *Environ. Sci. Technol.* **2021**, *55*, 10224–10230. [CrossRef] [PubMed]
9. Liang, S.; Elsworth, D.; Li, X.; Fu, X.; Sun, B.; Yao, Q. Key strata characteristics controlling the integrity of deep wells in longwall mining areas. *Int. J. Coal Geol.* **2017**, *172*, 31–42. [CrossRef]
10. Han, H.; Liang, S.; Liang, Y.; Fu, X.; Kang, J.; Yu, L.; Tang, C. The Role of Coal Mechanical Characteristics on Reservoir Permeability Evolution and Its Effects on CO2 Sequestration and Enhanced Coalbed Methane Recovery. *Geofluids* **2020**, *2020*, 8842309. [CrossRef]

11. Ajayi, K.M.; Schatzel, S.J. Transport model for shale gas well leakage through the surrounding fractured zones of a longwall mine. *Int. J. Min. Sci. Technol.* **2020**, *30*, 635–641. [CrossRef] [PubMed]
12. Su, D.W.H. Effects of longwall-induced stress and deformation on the stability and mechanical integrity of shale gas wells drilled through a longwall abutment pillar. *Int. J. Min. Sci. Technol.* **2017**, *27*, 115–120. [CrossRef]
13. Peng, S.S.; Cheng, J.; Du, F.; Xu, Y. Underground ground control monitoring and interpretation, and numerical modeling, and shield capacity design. *Int. J. Min. Sci. Technol.* **2019**, *29*, 79–85. [CrossRef]
14. Xu, Y.; Liang, S.; Liang, X.; Yang, B.; Shi, Z.; Wu, C.; Shen, J.; Yang, M.; Ma, Y.; Xu, P. Spatio-Temporal Evolution of Loading and Deformation of Surface Gas Pipelines for High-Intensity Coalbed Mining and Its Integrity Prediction Methodology. *Processes* **2024**, *12*, 213. [CrossRef]
15. Liang, S.; Elsworth, D.; Fu, X.; Li, X.; Yao, Q. Influence of Stratigraphic Conditions on the Deformation Characteristics of Oil/Gas Wells Piercing Longwall Pillars and Mining Optimization. *Energies* **2017**, *10*, 775. [CrossRef]
16. Cui, X.J.; Bustin, R.M. Volumetric strain associated with methane desorption and its impact on coalbed gas production from deep coal seams. *Aapg Bull.* **2005**, *89*, 1181–1202. [CrossRef]
17. Cui, X.; Bustin, R.M.; Chikatamarla, L. Adsorption-induced coal swelling and stress: Implications for methane production and acid gas sequestration into coal seams. *J. Geophys. Res. Solid Earth* **2007**, *112*, 1–16. [CrossRef]
18. Wang, J.G.; Liu, J.; Kabir, A. Combined effects of directional compaction, non-Darcy flow and anisotropic swelling on coal seam gas extraction. *Int. J. Coal Geol.* **2013**, *109*, 1–14. [CrossRef]
19. Rice, A.K.; McCray, J.E.; Singha, K. Methane Leakage from Hydrocarbon Wellbores into Overlying Groundwater: Numerical Investigation of the Multiphase Flow Processes Governing Migration. *Water Resour. Res.* **2018**, *54*, 2959–2975. [CrossRef]
20. Schout, G.; Griffioen, J.; Hassanizadeh, S.M.; de Lichtbuer, G.C.; Hartog, N. Occurrence and fate of methane leakage from cut and buried abandoned gas wells in the Netherlands. *Sci. Total Environ.* **2019**, *659*, 773–782. [CrossRef]
21. Skrzypkowski, K.; Zagórski, K.; Zagórska, A. Determination of the Extent of the Rock Destruction Zones around a Gasification Channel on the Basis of Strength Tests of Sandstone and Claystone Samples Heated at High Temperatures up to 1200 °C and Exposed to Water. *Energies* **2021**, *14*, 6464. [CrossRef]
22. Huo, B.; Jing, X.; He, A.; Fan, C. Hydraulic-Mechanical Coupling Model with Dual-Porosity Dual-Permeability for Anisotropy Coal Seams and Its Application in Mine Gas Extraction. *Adv. Civ. Eng.* **2019**, *2019*, 4534835. [CrossRef]
23. Ren, C.; Li, B.; Xu, J.; Wang, Z.; Li, J.; Zhang, Y.; Yu, J. Coal permeability evolution during damage process under different mining layouts. *Energy Sources Part A Recovery Util. Environ. Eff.* **2020**, 1–16. [CrossRef]
24. Li, Y.; Wang, Z.; Tang, S.; Elsworth, D. Re-evaluating adsorbed and free methane content in coal and its ad- and desorption processes analysis. *Chem. Eng. J.* **2022**, *428*, 131946. [CrossRef]
25. Gao, Q.; Liu, J.; Huang, Y.; Li, W.; Shi, R.; Leong, Y.; Elsworth, D. A critical review of coal permeability models. *Fuel* **2022**, *326*, 125124. [CrossRef]
26. Moortgat, J.; Schwartz, F.W.; Darrah, T.H. Numerical Modeling of Methane Leakage from a Faulty Natural Gas Well into Fractured Tight Formations. *Groundwater* **2018**, *56*, 163–175. [CrossRef] [PubMed]
27. Li, S.; Fan, C.; Han, J.; Luo, M.; Yang, Z.; Bi, H. A fully coupled thermal-hydraulic-mechanical model with two-phase flow for coalbed methane extraction. *J. Nat. Gas. Sci. Eng.* **2016**, *33*, 324–336. [CrossRef]
28. Zhu, W.C.; Liu, J.; Sheng, J.C.; Elsworth, D. Analysis of coupled gas flow and deformation process with desorption and Klinkenberg effects in coal seams. *Int. J. Rock. Mech. Min.* **2007**, *44*, 971–980. [CrossRef]
29. Khanal, M.; Qu, Q.; Zhu, Y.; Xie, J.; Zhu, W.; Hou, T.; Song, S. Characterization of Overburden Deformation and Subsidence Behavior in a Kilometer Deep Longwall Mine. *Minerals* **2022**, *12*, 543. [CrossRef]
30. He, M.; Wang, Q. Rock dynamics in deep mining. *Int. J. Min. Sci. Technol.* **2023**, *33*, 1065–1082. [CrossRef]

Disclaimer/Publisher's Note: The statements, opinions and data contained in all publications are solely those of the individual author(s) and contributor(s) and not of MDPI and/or the editor(s). MDPI and/or the editor(s) disclaim responsibility for any injury to people or property resulting from any ideas, methods, instructions or products referred to in the content.